

Stress wave propagation in 1-D and 2-D media using Smooth Particle Hydrodynamics method

Z. S. Liu[†]

*Computational Mechanics Division, Institute of High Performance Computing,
1 Science Park Road, #01-01 The Capricorn, Singapore Science Park II, Singapore, 117528*

S. Swaddiwudhipong[‡] and C. G. Koh^{‡†}

*Department of Civil Engineering, The National University of Singapore,
10 Kent Ridge Crescent Singapore, 119260*

(Received May 21, 2002, Accepted September 2, 2002)

Abstract. The paper involves the study on the elastic and elasto-plastic stress wave propagation in the 1-D and 2-D solid media. The Smooth Particle Hydrodynamics equations governing the elastic and elasto-plastic large deformation dynamic response of solid structures are presented. The proposed additional stress points are introduced in the formulation to mitigate the tensile instability inherent in the SPH approach. Both incremental rate approach and leap-frog algorithm for time integration are introduced and the new solution algorithm is developed and implemented. Two examples on stress wave propagation in aluminium bar and 2-D elasto-plastic steel plate are included. Results from the proposed SPH approach are compared with available analytical values and finite element solutions. The comparison illustrates that the stress wave propagation problems can be effectively solved by the proposed SPH method. The study shows that the SPH simulation is a reliable and robust tool and can be used with confidence to treat transient dynamics such as linear and non-linear transient stress wave propagation problems.

Key words: dynamic response; elastic and elasto-plastic materials; large deformation; Smooth Particle Hydrodynamics; stress point approach; stress wave propagation; tensile instability.

1. Introduction

Wave propagation is an important topic in engineering sciences, especially, in the field of solid mechanics. In solid mechanics, there are two types of stress waves (i) the compression wave and (ii) the shear wave. Due to continual reflection at boundaries and the propagation of waves in bounded solid, a steady state is usually finally reached. Depending on the influence of the inertia term, this state is governed by a static and dynamic equilibrium in frequency domain. However, if the rate of onset of the load is high compared to the time needed to reach this steady state, wave

[†]Senior Research Engineer

[‡] Deputy Head (Academic)

^{‡†} Deputy Head (Research)

propagation phenomena have to be considered. Applications of wave phenomena can be found in nearly every field of engineering. Some examples include the design of defence structures, blasting of rock and the destructive waves produced by earthquake. Knowledge on wave propagation phenomenon and its amplitude is imperative for preventive design of structures from destruction under impulse loading.

Only a few simple stress wave propagation problems can be solved analytically (Graff 1975). In most cases especially in 2-D and 3-D non-linear problems, the solutions are obtained through numerical analysis. So far, the Finite Element Method (FEM) has been widely used to solve various non-linear stress wave propagation problems. However, one of the main drawbacks of the FEM is the need to re-mesh to avoid the severe element distortions. Unfortunately, the re-meshing procedure introduces projection error and reduces the accuracy of the numerical solutions. In order to mitigate this cause of inaccuracy, a meshless method (or particle method) such as Smooth Particle Hydrodynamics (SPH) approach has been developed to solve the large deformation problems in solid mechanics.

SPH is a meshless method that offers considerable promise as a numerical tool for modeling problems involving large deformations and large distortions whereby the motion of a discrete number of particles of a solid is followed in time. SPH, a pure Lagrangian particle method, was first introduced by Lucy (1977) and Gingold and Monaghan (1977) respectively. It was originally developed for treating astrophysics problems. The method was extended to solve solid mechanics problems (Libersky and Petschek 1991), hypervelocity impact problems (Libersky *et al.* 1993) and penetration problems. In SPH, the field variables such as velocity, density, deformation gradient and stresses are obtained from particle values using interpolation functions known as kernel function. As SPH uses a Lagrangian formulation for the equations of motion, it does not involve a distortion limiting grid and is therefore very attractive for any high velocity impact and transient dynamics simulation.

The advantage of the SPH method is that it is easy to work with and provides reasonably accurate results for solid mechanics problems. However, the method suffers the loss in accuracy and often the instability phenomenon resulting from the lack of nodal completeness and/or integrability of the kernel approximations. If explicit time integration scheme is adopted, SPH shares the basic Courant time step stability requirements for hydrodynamic analysis. Tensile instability is the main common problem associated with SPH for solids experiencing state of tensile stress. An improvement on completeness and integrability conditions as well as stability of the process is imperative for SPH to become a robust tool. Monaghan (1989), Johnson and Beissel (1996) and Randles and Libersky (1996) have proposed the correcting first derivative approximation method. Although these correction techniques can restore various levels of nodal completeness, none of them is truly complete as the integrability condition is not satisfied. In order to overcome tensile instability in SPH, Hicks *et al.* (1997) proposed the conservative smoothing method while Dyka and Ingel (1995) and Dyka *et al.* (1997) suggested the stress-point approach. Later, the SPH method has been extended to a stress-point formulation with boundary conditions by Randles and Libersky (2000). In their paper, the collocation nature of standard SPH is removed by adding a companion set of Lagrangian points that carry the stress. By using this stress point treatment, a stable and linearly consistent solution can be obtained. Recently, Chen *et al.* (1999a, 1999b, 2001) have proposed a simple corrective kernel approximation technique, which was called the Corrective Smoothed Particle Method (CSPM) by applying the kernel estimate to the Taylor series expansion. This solution algorithm is capable of solving time-dependent partial differential equations of any order.

As demonstrated by Chen *et al.* (1999a), the use of the corrective second derivative approximations can result in stable and accurate solutions. For linear elasto-dynamics, the Corrective Smoothed Particle Method with the corrective first derivative approximations not only can remove the tensile instability in SPH but also can enhance solution accuracy over the entire domain, especially near and on boundaries (Chen *et al.* 1999b). Belytschko *et al.* (1998) showed that for the case of nodal quadrature, the element-free Galerkin solutions even with an integrable test function would exhibit marked numerical instability. They found that the instability of solutions could be prevented by the conservative smoothing technique of Randles and Libersky (1996) while dynamic solution instability, if occurred, could be stabilised by the introduction of artificial viscosity (Monaghan and Gingold 1983).

The Smooth Particle Hydrodynamics equations governing the elasto-plastic large deformation dynamic response of solids are presented. The proposed additional stress points are introduced in the formulation to treat tensile instability. Furthermore, in order to increase the accuracy of SPH solutions, the incremental rate approach of SPH method suitable and effective for large deformation stress wave propagation was proposed. Combining the incremental rate approach with standard leap-frog algorithm for time integration, the new solution algorithm was developed. Several examples covering the stress wave propagation in 1-D and 2-D elastic and elasto-plastic media are presented. Comparison of results demonstrates the validity and stability of the proposed approach.

2. Smooth Particle Hydrodynamics

In Smooth Particle Hydrodynamics method, a continuum is represented by a set of points or particles. The foundation of SPH is the interpolation theory. Through the use of kernel estimates, the partial differential equations can be transformed into integral forms. Numerically, these integral equations are approximated in terms of the field variables at a set of discrete points or particles. These field variables are then directly evolved from the interactions among the particles using an explicit time integration scheme.

A kernel approximation for a function f representing a field variable at a particular point, whose position vector is $\mathbf{x} = (x^1, x^2, x^3)$, in a volume Ω can be expressed as

$$f(\mathbf{x}) \cong \int_{\Omega} f(\mathbf{x}') W(\mathbf{x} - \mathbf{x}'; h) d\mathbf{x}' \quad (1)$$

where $W(\mathbf{x} - \mathbf{x}'; h)$ is a kernel (or smooth) function; h is a measure of the width of the kernel; $d\mathbf{x}'$ is the differential volume. The kernel function is dependent upon two variables, $(\mathbf{x} - \mathbf{x}')$ and h , and has the following three special properties, i.e., 1) it has a compact support; 2) it reduces to the Dirac-delta function, when h approaches zero and 3) it is normalised (Swegle and Attaway 1995).

The formulation of derivative estimates in SPH includes integration by parts, neglecting residual boundary terms, and a linearization procedure that takes integrals of products equal to products of integrals and drops the kernel estimates for quantities that do not involve spatial derivatives. Through this technique and divergence theorem, the divergence estimates for a vector field f can be generated, i.e.,

$$\nabla \cdot f(\mathbf{x}) \cong - \int_{\Omega} f(\mathbf{x}') \cdot \nabla W(\mathbf{x} - \mathbf{x}'; h) d\mathbf{x}' \quad (2)$$

The kernel approximation allows spatial gradients to be determined from the derivative of the kernel rather than the derivative of the function itself.

As the state variables in SPH are known at discrete particle locations, integrals over a continuous volume are equivalent to the summation of the values of neighbour particles. Assuming the sum is over N interpolation points, Eqs. (1) and (2) become respectively

$$f(\mathbf{x}_i) \cong \sum_{j=1}^N f_j(\mathbf{x}_j) W(\mathbf{x}_i - \mathbf{x}_j; h) \frac{m_j}{\rho_j} \quad (3)$$

$$\nabla \cdot f(\mathbf{x}_i) \cong - \sum_{j=1}^N f_j(\mathbf{x}_j) \cdot \nabla W(\mathbf{x}_i - \mathbf{x}_j; h) \frac{m_j}{\rho_j} \quad (4)$$

The above equations provide continuous approximations to a function and its gradient based on an arbitrary set of discrete interpolation points at which the function is known. It is obvious from Eqs. (3) and (4) that SPH particles should be thought of as interpolation points with no connectivity or spatial relation among them. The sum is over the entire set of points, however, only those within the range of the kernel function will contribute. In order to avoid an algorithm in which distances between all particles are tested to establish those contributing to the sums, a search algorithm to find neighbours is adopted. Searching for the neighbour particles for each particle i is usually the most computationally intensive part in an SPH simulation. The present study adopts the linked list algorithm proposed by Hockney and Eastwood (1981). The method reduces significantly the computational cost.

Function f and its gradient at the position \mathbf{x}_i of the i^{th} particle can thus be expressed as

$$f_i = f(\mathbf{x}_i) \cong \sum_{j=1}^N f_j W_{ij} \frac{m_j}{\rho_j} \quad (5)$$

$$\nabla \cdot f(\mathbf{x}_i) \cong - \sum_{j=1}^N f_j \cdot \nabla W_{ij} \frac{m_j}{\rho_j} \quad (6)$$

in which the subscripts i and j represent the particle number; m_j and ρ_j are the mass and density of particle j ; N is the number of total particles in the field; $W_{ij} = W(\mathbf{x}_i - \mathbf{x}_j; h)$ and $\nabla \cdot W_{ij} = \partial W(\mathbf{x}_i - \mathbf{x}_j; h) / \partial \mathbf{x}_j$. Since $W_{ij} = 0$ for $|\mathbf{x} - \mathbf{x}'| \geq 2h$, N can be dually considered as the number of particles that effectively interact with particle i . This approximation to the field variables forms the basis of SPH.

Two other widely used SPH formulas (Benz 1990) for gradients are:

$$\nabla \cdot f(\mathbf{x}_i) = \frac{1}{\rho(\mathbf{x}_i)} \sum_{j=1}^N m_j (f(\mathbf{x}_i) - f(\mathbf{x}_j)) \cdot \nabla W_{ij} \quad (7)$$

$$\nabla \cdot f(\mathbf{x}_i) = -\rho_i \sum_{j=1}^N m_j \left(\frac{f(\mathbf{x}_i)}{\rho^2(\mathbf{x}_i)} - \frac{f(\mathbf{x}_j)}{\rho^2(\mathbf{x}_j)} \right) \cdot \nabla W_{ij} \quad (8)$$

To implement the SPH algorithm, the kernel function must be specified. Although a few possible kernel functions exist, one of the most efficient and widely used is the cubic B-spline kernel

$$W(r) = \begin{cases} \frac{C}{h^\lambda} \left(1 - \frac{3}{2}r^2 + \frac{3}{4}r^3 \right) & r < 1 \\ \frac{C}{4h^\lambda} (2-r)^3 & 1 \leq r < 2 \\ 0 & r > 2 \end{cases} \quad (9)$$

where $r = |\mathbf{x}_i - \mathbf{x}_j|$, $\lambda = 1, 2$ and 3 for 1-D, 2-D and 3-D problems respectively. The three values of the normalised constant C are $2/3, 10/(7\pi)$ and $1/\pi$, corresponding to the cases of $\lambda = 1, 2$ and 3 respectively.

The first and second derivatives of the B-spline kernel function can be expressed as:

$$W_{ij, \alpha} = \frac{\partial W_{ij}}{\partial x_j^\alpha} = \frac{dW_{ij}}{dr} \frac{\partial r}{\partial x_j^\alpha}, \quad (10)$$

$$W_{ij, \alpha\beta} = \frac{\partial W_{ij}}{\partial x_j^\alpha \partial x_j^\beta} = \frac{\partial r}{\partial x_j^\alpha} \left(\frac{d^2 W_{ij}}{dr^2} - \frac{1}{r} \frac{dW_{ij}}{dr} \right) \frac{\partial r}{\partial x_j^\beta} + \frac{\delta_{\alpha\beta}}{rh^2} \frac{dW_{ij}}{dr}, \quad (11)$$

with

$$\frac{\partial r}{\partial x_j^\alpha} = \frac{(x_j^\alpha - x_i^\alpha)}{h|x_j^\alpha - x_i^\alpha|}, \quad (12)$$

The distributions of the kernel function W , its first derivative dW/dr and its second derivative d^2W/dr^2 as shown in Fig. 1 show that W_{ij} and d^2W/dr^2 are symmetrical functions while the first derivative dW/dr is anti-symmetric.

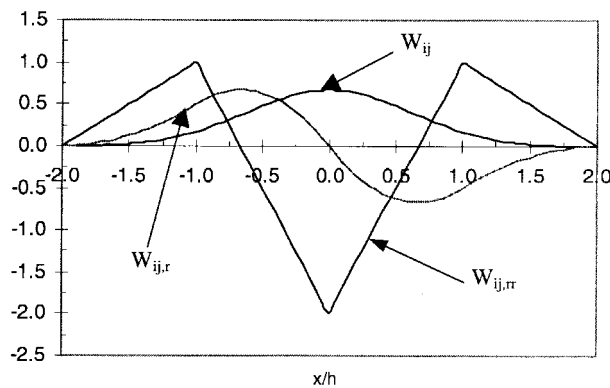


Fig. 1 Cubic spline kernel function and its derivatives

3. SPH approach in solid mechanics

3.1 Equations of motion

The differential equations for the conservation of mass, linear momentum and energy are expressed as:

$$\frac{d\rho}{dt} = \rho \frac{\partial v^\alpha}{\partial x^\alpha} \quad (13)$$

$$\frac{dv^\alpha}{dt} = \frac{1}{\rho} \frac{\partial \sigma^{\alpha\beta}}{\partial x^\beta} \quad (14)$$

$$\frac{dE}{dt} = \frac{\sigma^{\alpha\beta} \partial v^\alpha}{\rho \partial x^\beta} \quad (15)$$

where $dx^\alpha/dt = v^\alpha$, the v^α is the velocity components, $\sigma^{\alpha\beta}$ is the stress tensor, E is the energy, ρ is the density. The independent variables are spatial co-ordinates x^α and time t . Various SPH forms of conservation equations can be produced through the introduction of Eqs. (5) to (8) into Eqs. (13) to (15) and integration by parts.

$$\frac{d\rho_i}{dt} = \rho_i \sum_j \frac{m_j}{\rho_j} (v_i^\beta - v_j^\beta) \frac{\partial W_{ij}}{\partial x^\beta} \quad (16)$$

$$\frac{dv_i^\alpha}{dt} = \sum_j m_j \left(\frac{\sigma_i^{\alpha\beta}}{\rho_i^2} + \frac{\sigma_j^{\alpha\beta}}{\rho_j^2} \right) \frac{\partial W_{ij}}{\partial x^\beta} \quad (17)$$

$$\frac{dE_i}{dt} = \frac{\sigma_i^{\alpha\beta}}{\rho_i^2} \sum_j m_j (v_j^\alpha - v_i^\alpha) \frac{\partial W_{ij}}{\partial x^\beta} \quad (18)$$

The superscripts α and β indicate the components of the vector quantities. Summation over the repeated indices is implied. The total time derivative, $d()/dt$, is taken in the Lagrangian frame. For given particle i the density change acceleration and change in internal energy are given by Eqs. (16) to (18) respectively.

3.2 Artificial viscosity

In SPH, artificial viscosity and heat flux are often employed to overcome the numerical instability caused by shock waves (Libersky *et al.* 1993). The artificial viscous pressure used in this study was developed by Monaghan and Gingold (1983) and is expressed as:

$$\Pi_{ij} = \begin{cases} \frac{-\zeta \bar{c}_{ij} \mu_{ij} + \eta \mu_{ij}^2}{\rho_{ij}} & \text{if } (\mathbf{v}_i - \mathbf{v}_j) \cdot (\mathbf{x}_i - \mathbf{x}_j) < 0 \\ 0 & \text{otherwise} \end{cases} \quad (19)$$

where

$$\mu_{ij} = \frac{h(\mathbf{v}_i - \mathbf{v}_j) \cdot (\mathbf{x}_i - \mathbf{x}_j)}{|\mathbf{x}_i - \mathbf{x}_j|^2 + kh^2} \quad (20)$$

$$\bar{c}_{ij} = (c_i + c_j)/2, \quad \bar{\rho}_{ij} = (\rho_i + \rho_j)/2 \quad (21)$$

in which, c is the sound speed on particle i , ζ and η are constants and k is usually taken as 0.1. The linear term in Eq. (19) produces a shear and bulk viscosity while the quadratic term is roughly equivalent to the Von Neumann-Richtmyer viscosity. If the artificial viscous functions are introduced into the momentum equations, Eqs. (16) to (18) become

$$\frac{d\rho_i}{dt} = \rho_i \sum_j \frac{m_j}{\rho_j} (v_i^\beta - v_j^\beta) \frac{\partial W_{ij}}{\partial x^\beta} \quad (22)$$

$$\frac{du_i^\alpha}{dt} = \sum_j m_j \left(\frac{\sigma_i^{\alpha\beta}}{\rho_i^2} + \frac{\sigma_j^{\alpha\beta}}{\rho_j^2} + \Pi_{ij} \right) \frac{\partial W_{ij}}{\partial x^\beta} \quad (23)$$

$$\frac{dE_i}{dt} = \sum_j m_j (v_j^\alpha - v_i^\alpha) \left(\frac{\sigma_i^{\alpha\beta}}{\rho_i^2} + \frac{1}{2} \Pi_{ij} \right) \frac{\partial W_{ij}}{\partial x^\beta} \quad (24)$$

3.3 Constitutive equation

In hydrodynamic analysis, the stress tensor appearing in the conservation equations is defined as functions of the hydrostatic pressure $P = -1/3 \text{Tr}(\sigma)$ and the traceless symmetric deviatoric stress S as

$$\sigma = S - PI \quad \text{or} \quad \sigma^{\alpha\beta} = S^{\alpha\beta} - P\delta_{\alpha\beta} \quad (25)$$

In classical plasticity, hydrostatic pressure P is usually calculated using the linear Hooke's law when P is small. For severe hydrostatic pressure, the pressure should be evaluated with Equation of State (EOS) having the functional $P = P(\rho, E)$. The EOS employed in this study is the well-known Mie-Gruneisen EOS for solids (Libersky *et al.* 1993, Drumheller 1998).

$$P(\rho, E) = \left(1 - \frac{1}{2} \Gamma \eta \right) P_H(\rho) + \Gamma \rho E \quad (26)$$

$$P_H = \begin{cases} a_1 \eta + \alpha_2 \eta^2 + a_3 \eta^3 & \eta > 0 \\ a_1 \eta & \eta < 0 \end{cases} \quad (27)$$

where $\eta = \rho/\rho^0 - 1$ and the subscript H refers to Hugoniot curve representing compression and Γ is the Gruneisen constant of material. The constants, a_1 to a_3 , can be related to parameters c and s in linear shock velocity-particle velocity relation $v_s = c + sv_p$ through the Taylor's series expansion of the Hugoniot function expressed as:

$$a_1 = \rho_0 c^2, \quad a_2 = a_1[1 + 2(s-1)], \quad a_3 = a_1[2(s-1) + 3(s-1)^2] \quad (28)$$

in which s is the slope of the approximate linear relationship between the shock velocity (v_s) and particle velocity (v_p), and c is the sound speed of the material. The details are given in Drumheller (1998). In this study, the EOS will be determined by the conservation of mass, balance of linear momentum and linear-Hugoniot relationship and Eq. (26) is simplified to

$$p(\rho, E) = \left(1 - \frac{1}{2}\Gamma\eta\right)p_H(\rho). \quad (29)$$

In the elastic range, the deviatoric stress rate can be determined through Hooke's law

$$\dot{S} = 2G\dot{\epsilon}' \quad (30)$$

where G is the shear modulus and $\dot{\epsilon}' = \dot{\epsilon} - 1/3Tr(\dot{\epsilon})I$ is deviatoric strain rate tensor. For finite rotation, the deviatoric stress should be determined through the incremental plasticity theory. To account for the large rotation effect, the elastic deviatoric stress rate, $\dot{S}^{\alpha\beta}$, is computed using the Jaumann rate definition:

$$\dot{S}^{\alpha\beta} = 2G\left(\dot{\epsilon}^{\alpha\beta} - \frac{1}{3}\delta^{\alpha\beta}\dot{\epsilon}^{\gamma\gamma}\right) + S^{\alpha\gamma}\Omega^{\beta\gamma} + S^{\gamma\beta}\Omega^{\alpha\gamma} \quad (31)$$

where

$$\dot{\epsilon}^{\alpha\beta} = \frac{1}{2}\left(\frac{\partial v^\alpha}{\partial x^\beta} + \frac{\partial v^\beta}{\partial x^\alpha}\right) \quad \text{and} \quad \Omega^{\alpha\beta} = \frac{1}{2}\left(\frac{\partial v^\alpha}{\partial x^\beta} - \frac{\partial v^\beta}{\partial x^\alpha}\right) \quad (32)$$

are the strain rate and rotation rate tensors, respectively. Using particle equation, the SPH expressions for evaluating these two tensors are derived as

$$\dot{\epsilon}_i^{\alpha\beta} = \frac{1}{2}\sum_j \frac{m_j}{\rho_j} [(v_j^\alpha - v_i^\alpha)W_{ij,\beta} + (v_j^\beta - v_i^\beta)W_{ij,\alpha}] \quad (33)$$

$$\Omega_i^{\alpha\beta} = \frac{1}{2}\sum_j \frac{m_j}{\rho_j} [(v_j^\alpha - v_i^\alpha)W_{ij,\beta} - (v_j^\beta - v_i^\beta)W_{ij,\alpha}] \quad (34)$$

In view of Eq. (16), Eq. (33) becomes

$$\dot{\epsilon}_i^{\gamma\gamma} = \sum_j \frac{m_j}{\rho_j} (v_j^\gamma - v_i^\gamma)W_{ij,\gamma} = \frac{\dot{\rho}_i}{\rho_i} \quad (35)$$

Therefore Eq. (31) can be rewritten as

$$\begin{aligned} & \dot{S}_i^{\alpha\beta} - S_i^{\alpha\gamma}\Omega^{\beta\gamma} - S_i^{\gamma\beta}\Omega^{\alpha\gamma} \\ &= G\sum_j \frac{m_j}{\rho_j} \left[(v_j^\alpha - v_i^\alpha)W_{ij,\beta} + (v_j^\beta - v_i^\beta)W_{ij,\alpha} - \frac{2}{3}\delta^{\alpha\beta}\frac{\dot{\rho}_i}{\rho_i} \right] \end{aligned} \quad (36)$$

3.4 Tension instability treatment

Standard SPH methods have been plagued by a serious problem referred to as tension instability.

It is imperative to search for a suitable method to treat this problem. Sweigle *et al.* (1995) carried out a formal stability analysis and discussed the roots of tension instability. In essence, standard SPH simulation may result in a premature fracture in tension. In 1-D problems, tension instability will cause the simple elastic bar to break apart in tension (Dyka *et al.* 1995 & 1997). For 2-D and 3-D problems, tension instability will produce a clustering of particles which may lead to a premature fracture. Dyka *et al.* (1997) proposed a stress point method to treat this problem. Its main idea is that the stresses are calculated at points other than the SPH centroids in order to remove the instability. This approach completely eliminates tension instability for a 1-D bar producing very accurate solutions for several SPH formulations. However, their study did not cover 2-D and 3-D problems. Randles and Libersky (2000) have extended SPH to a normalized, staggered particle formulation with boundary conditions. In their study, a companion set of interpolation points is introduced that carry stress, velocity gradient, and other field variables. The proposed method is shown to be stable and linearly consistent.

The concept of stress points of Dyka is adopted and expanded to cover 2-D and 3-D problems in particular to plate and shell structures. The stress-point method for SPH is analogous to full integration in FEA, and staggered finite difference schemes. For standard SPH, the stress components are calculated at the centroid of the SPH particle analogous to a reduced integration form of FEA. Fig. 2 illustrates the typical SPH particles based on the stress point approach. The stress points are symmetrically shifted away from the centre of the particle by a parametric distance μ . $\mu = 1$ indicates the stress points at the boundaries while $\mu = 0$ corresponds to the standard form of SPH where stress point is located at the centroid of each particle. In this approach, stress, internal energy, and density are calculated and tracked at the stress points while the displacement, velocity and acceleration are all calculated and monitored at the centroid of each particle.

The formulation of the conservation equation can be derived based on the stress point approach and the momentum equation, Eq. (17), can be expressed as

$$\frac{dv_i^\alpha}{dt} = \sum_j \sum_{l=1,2,\dots,8} m_{jl} \left(\frac{\sigma_i^{\alpha\beta}}{\rho_i^2} + \frac{\sigma_{jl}^{\alpha\beta}}{\rho_{jl}^2} \right) \frac{\partial W_{ij}}{\partial x^{\beta l}} \tag{37}$$

in which $l = 1$ to 8, $l = 1$ to 4 and $l = 1$ & 2 correspond to the eight, four and two stress points for

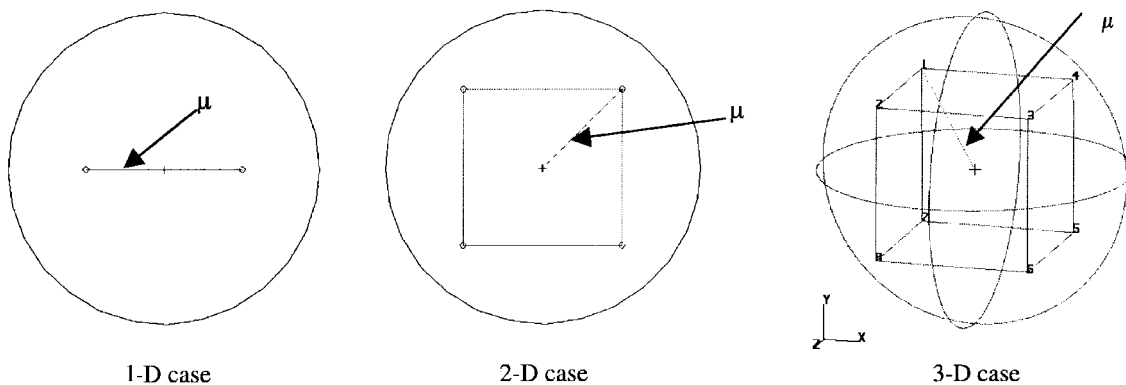


Fig 2 Typical SPH particles for the stress point method

3-D, 2-D and 1-D problems respectively as shown in Fig. 2. In addition, one-eighth the mass, one-fourth the mass and half the mass of particle j is assigned to each stress point. The stress at the centroid of particle i , $\sigma_i^{\alpha\beta}$ can be approximated to be

$$\begin{aligned}\sigma_i^{\alpha\beta} &\approx \frac{1}{8} \sum_l^8 \sigma_i^{\alpha\beta l} \quad \text{for 3-D case} \\ \sigma_i^{\alpha\beta} &\approx \frac{1}{4} \sum_l^4 \sigma_i^{\alpha\beta l} \quad \text{for 2-D case} \\ \sigma_i^{\alpha\beta} &\approx \frac{1}{2} \sum_l^2 \sigma_i^{\alpha\beta l} \quad \text{for 1-D case}\end{aligned}\quad (38)$$

As the stress tensors in particle i are included in the linear momentum equation of the same particle, the tension instability is eliminated, accuracy of the results improved and undesirable oscillations mitigated.

4. Large deformation elasto-plastic dynamics

As large deformation elasto-plastic transient dynamic analysis is path-dependent, the incremental procedure is adopted. The strategy is to develop the solution process for the next required equilibrium position corresponding to time $t + \Delta t$ when the values of kinematic variables at all time steps from 0 to time t are known. The conservation equations of solid mechanics at time $t + \Delta t$ can be obtained from Eqs. (13) and (15) as

$$\frac{d^{t+\Delta t} \rho_i}{dt} = {}^{t+\Delta t} \rho_i \frac{\partial^{t+\Delta t} v_i^\alpha}{\partial x^\alpha} \quad (39)$$

$$\frac{d^{t+\Delta t} v_i^\alpha}{dt} = \frac{1}{{}^{t+\Delta t} \rho_i} \frac{\partial^{t+\Delta t} \sigma_i^{\alpha\beta}}{\partial x^\beta} \quad (40)$$

$$\frac{d^{t+\Delta t} E_i}{dt} = \frac{{}^{t+\Delta t} \sigma_i^{\alpha\beta} \partial^{t+\Delta t} v_i^\alpha}{{}^{t+\Delta t} \rho_i \partial x^\beta} \quad (41)$$

Let ${}^{t+\Delta t} \sigma_i^{\alpha\beta}$ be the increment of stresses of particle i from time t to $t + \Delta t$ with the following relation

$${}^{t+\Delta t} \sigma_i^{\alpha\beta} = {}^t \sigma_i^{\alpha\beta} + {}^{t+\Delta t} \sigma_i^{\alpha\beta} \quad (42)$$

Therefore Eq. (40) becomes

$${}^{t+\Delta t} \rho_i \frac{d^{t+\Delta t} v_i^\alpha}{dt} = {}^t \rho_i \frac{d^t v_i^\alpha}{dt} + \frac{\partial^{t+\Delta t} \sigma_i^{\alpha\beta}}{\partial x^\beta} \quad (43)$$

Essential effort for solving Eq. (43) is to establish the stress increment gradients $\frac{\partial^{t+\Delta t} \sigma_i^{\alpha\beta}}{\partial x^\beta}$.

4.1 Large deformation elastic case

The incremental stresses can be expressed in terms of incremental strains. In the hydro-dynamics analysis, the incremental stress can be defined in terms of hydrostatic pressure and traceless symmetric deviatoric stress:

$${}^{t+\Delta t} \sigma_i^{\alpha\beta} = {}^{t+\Delta t} S_i^{\alpha\beta} - P \delta_{\alpha\beta} \quad \text{and} \quad p = -\frac{1}{3} {}^{t+\Delta t} \sigma_i^{\gamma\gamma} \quad (44)$$

The incremental deviatoric stress, ${}^{t+\Delta t} S_i^{\alpha\beta}$, is computed using the Jaumann rate definition as stated in Eq. (31).

4.2 Elasto-plastic materials

For elasto-plastic small strain case, the incremental stress can be expressed as functions of incremental strain in an average sense (Chen *et al.* 2001). In this situation, the constitutive equation can be given by

$${}^{t+\Delta t} \sigma_i^{\alpha\beta} = {}^{t+\Delta t} C_{\alpha\beta\gamma\delta} {}^{t+\Delta t} \epsilon_i^{\gamma\delta} \quad (45)$$

where ${}^{t+\Delta t} C_{\alpha\beta\gamma\delta}$ are elastic-plastic stiffness coefficients during the time interval $(t, t + \Delta t)$. The detailed derivation of the elasto-plastic stiffness coefficients can be found in Owen and Hinton (1980).

Based on the Von-Mises assumption that plastic flow depends only on the deviatoric stress, the Von Mises J_{II} criterion and the associated flow rule are adopted to describe the plastic deformation in this type of materials.

$$J_{II} = {}^{t+\Delta t} S^{\alpha\beta} {}^{t+\Delta t} S^{\alpha\beta} \quad (46)$$

With J_{II} and yield stress σ_y , the deviatoric stress can be limited to the Von-Mises yield surface.

5. Time integration in SPH

An explicit central difference method can be used in the time integration process. Though many possible time integration schemes exist, the most common and simple procedures adopted in SPH literature are leap-frog explicit process (Monaghan 1985) and the predictor-corrector method (Monaghan 1989). Both conserve linear and angular momentum exactly.

The field variables in the SPH equations are directly updated using an explicit, leap-frog time integration algorithm. The magnitude of each time step Δt is controlled by the Courant-Friedrichs-Lewy (CFL) condition (Libersky *et al.* 1993).

$$\Delta t = C_{FL} \frac{h}{c + v_p} \quad (47)$$

C_{FL} is usually set to 0.3, c the sound speed and v_p the particle velocity. For a standard leap-frog scheme, the intermediate velocity vector at a field point i is defined as:

$${}^{t+0.5\Delta t}v_i^\alpha = {}^{t-0.5\Delta t'}v_i^\alpha + \frac{1}{2}(\Delta t + \Delta t')\frac{d {}^t v_i^\alpha}{dt} \tag{48}$$

where Δt and $\Delta t'$ are current and previous time step increment respectively. $d {}^t v_i^\alpha / dt$ is the acceleration vector at the point computed using the equilibrium equation at time t . The vector can be obtained through particle equation, Eq. (40), and the particle positions are updated to

$${}^{t+\Delta t}x_i^\alpha = {}^t x_i^\alpha + \Delta t {}^{t+0.5\Delta t}v_i^\alpha \tag{49}$$

The other variables at time $t + \Delta t$ can be updated to:

$${}^{t+\Delta t}\rho_i = {}^t\rho_i + \frac{d}{{}^t dt}({}^{t+\Delta t}\rho_i) \cdot \Delta t \tag{50}$$

$${}^{t+\Delta t}E = {}^tE + \frac{d}{{}^t dt}({}^{t+\Delta t}E) \cdot \Delta t \tag{51}$$

$${}^{t+\Delta t}S_i^{\alpha\beta} = {}^tS_i^{\alpha\beta} + \frac{d}{{}^t dt}({}^{t+\Delta t}S_i^{\alpha\beta}) \cdot \Delta t \tag{52}$$

The density rate, internal energy rate and stress rate can be evaluated from the particle equations.

6. Numerical examples

6.1 Wave propagation in an aluminium rod

The first example involves the study on the wave propagation in an aluminium rod. The problem description, geometry and material properties are given in Fig. 3 and Table 1. The rod is fixed at one end, and excited by a pressure jump according to a unit step function $P_x = 100 \text{ MPa } H(t)$ at its loaded end. The remaining surfaces are traction free. The material is assumed to be elastic and the Poisson's ratio is neglected to enable the comparison of results with existing 1-D longitudinal wave. According to Graffi (1954), the displacement and the normal stress in the 1-D rod can be expressed as

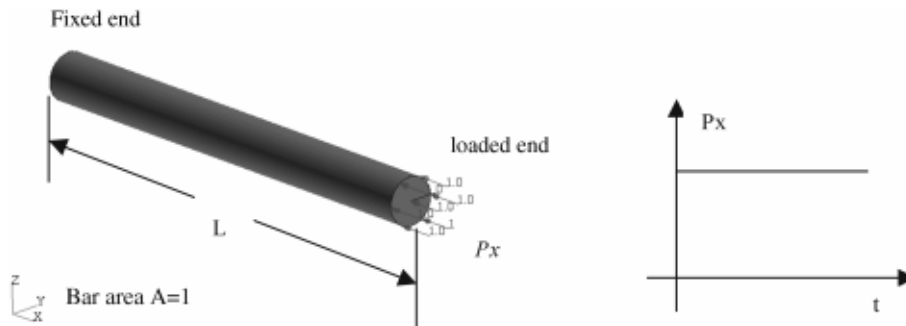


Fig. 3 Aluminum rod subjected to step function excitation at loaded end

Table 1 Material properties and geometry data of the rod

Young's modulus of elasticity	$E = 70. \times 10^3$ MPa
Poisson's ratio	$\nu = 0.$
Mass density	$\rho = 0.0027$ g/mm ³
Length of rod	$L = 10$ mm.
Rod section area	$A = 1$ mm ²

$$u(x, t) = \frac{P_x}{\rho c} \sum_{n=0}^{\infty} (-1)^n \left[\left(t - \frac{(2n+1)L-x}{c} \right) H \left(t - \frac{(2n+1)L-x}{c} \right) - \left(t - \frac{(2n+1)L+x}{c} \right) H \left(t - \frac{(2n+1)L+x}{c} \right) \right] \quad (53)$$

$$\sigma(x, t) = P_x \sum_{n=0}^{\infty} (-1)^n \left[H \left(t - \frac{(2n+1)L-x}{c} \right) + H \left(t - \frac{(2n+1)L+x}{c} \right) \right] \quad (54)$$

in which L denotes the length of the rod and the 1-D wave velocity is $c = \sqrt{E/\rho}$. $H(t)$ is the Heaviside step function and has the following properties.

$$H(t) = \begin{cases} 1 & \text{if } t \geq 0 \\ 0 & \text{if } t < 0 \end{cases} \quad (55)$$

In SPH simulation, the particles are placed along 1-D line to represent the 1-D bar, as shown in Fig. 4. To study the effects of number of particles on the convergence of the results, 3 set of particles are chosen to model the bar. They are 26, 51 and 101 particles with the smoothing length of each particle taken as 0.4 mm, 0.2 mm and 0.1 mm respectively. The time step is chosen as 2.5 nano-second and the artificial viscosity suggested by Monaghan and Gingold (1983) was introduced before the completion of the 2nd cycle. The adopted value of 2.5 nano-second is smaller than the critical value given by Eq. (47) to ensure convergence of the time integration.

Both numerical and analytical results are normalised by their corresponding static values, namely, the displacement $u_{sta} = 0.01428$ mm and the traction, $\sigma_{sta} = 100$ MPa. The normalised displacement history at the rod's loaded end and traction history at the fixed end are depicted in Figs. 5 and 6 respectively. In comparison with Graffi's results, they are in good agreement especially during the

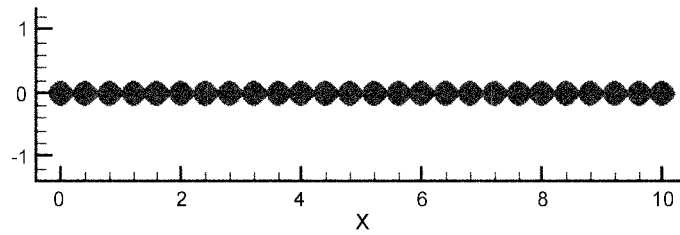


Fig. 4 SPH model for aluminum rod

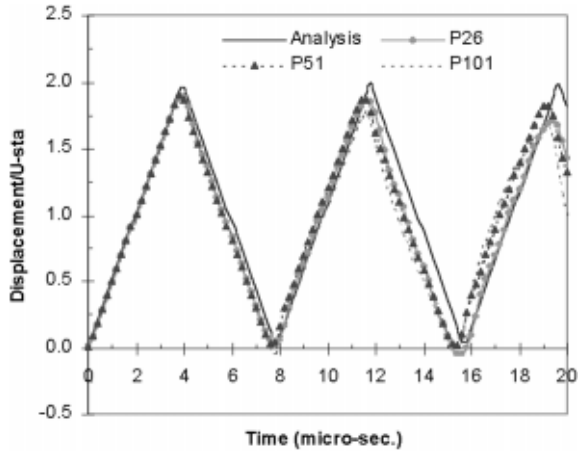


Fig. 5 Displacement history at loaded end for different numbers of particles

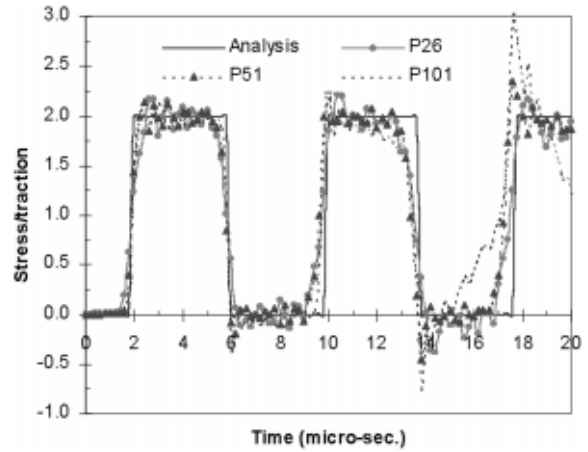


Fig. 6 Stress history at fixed end for different numbers of particles

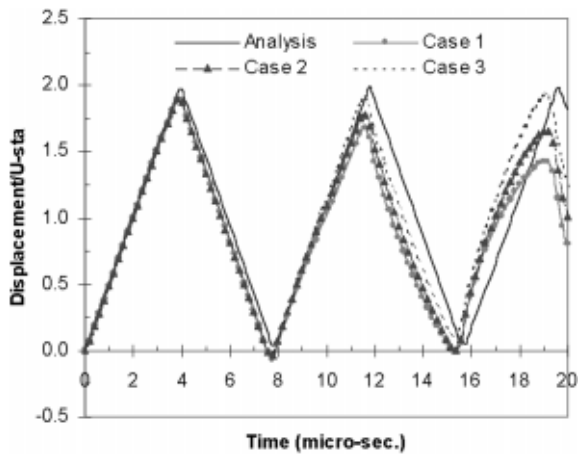


Fig. 7 Displacement history at loaded end for different time increments and artificial viscosity

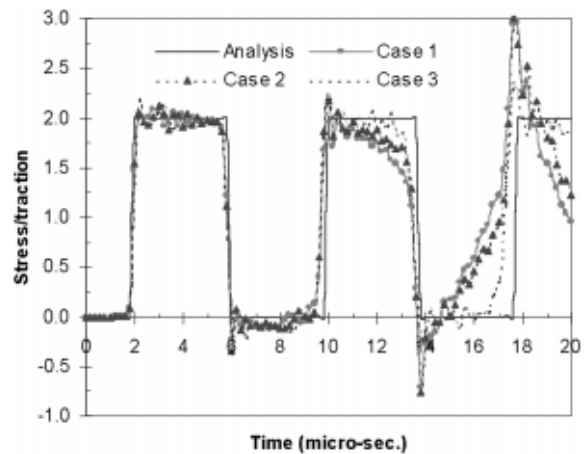


Fig. 8 Stress history at fixed end for different time increments and artificial viscosity

first 2 cycles. However, oscillation of stress wave is observed afterwards for model with 101 particles. The latter is most likely caused by accumulation of computational error. Three cases are considered to study the effects of size of the time step and artificial viscosity introduced to mitigate undesirable noises, They are Case 1: $\Delta t = 5$ nanosecond, Case 2: $\Delta t = 2.5$ nanosecond and Case 3: $\Delta t = 2.5$ nanosecond incorporating artificial viscosity given by Monaghan and Gingold (1983). All these values are smaller than the critical value obtained from Eq. (47). Both displacement and stress histories of the rod from the above 3 cases are depicted and compared with existing analytical results in Figs. 7 and 8 respectively. Comparison of results show good agreement especially during the first 2 cycles and the introduced artificial viscosity is effective in the reduction of undesirable noises at later stages.

6.2 Plane stress elasto-plastic wave propagation in rectangular steel plate

In this example, a rectangular steel plate subjected to a suddenly applied pressure load in x direction along its edges as indicated in Fig. 9, is used to verify the linear and nonlinear wave propagation and dynamic response of the proposed SPH approach. The plate is constrained in the x -direction along the left edge ($x=0$) and excited by a pressure jump of a unit step function $P_x = 150 \text{ N/mm}^2 H(t)$ on the loaded edge. The remaining surfaces of the plate are traction free. The properties of materials and geometry data of the steel plate are given in Table 2.

Both elastic and elasto-plastic dynamic analyses using SPH and finite element methods (Swaddiwudhipong and Liu 1996) have been carried out. In the latter, 8 quadratic shell elements are used to idealise the plate with the time increment, Δt , of $1.0 \mu\text{sec}$. For SPH, three different types of particle models are adopted in order to study the convergence of the problem. They are Type 1 : 51×26 , Type 2 : 101×51 and Type 3 : 201×101 2-D particle models with the smoothing lengths of 4.0 mm, 2.0 mm and 1.0 mm and the time steps of $0.4 \mu\text{sec}$, $0.2 \mu\text{sec}$, and $0.1 \mu\text{sec}$, respectively. Parametric studies show that for Type 1 model, even with reduced time-step increment, results are not acceptable as oscillation is prominently apparent even during the early stage of response. However, no significant discrepancy is observed from results of Types 2 and 3 SPH models indicating convergence of results when 101×51 2-D particle model is adopted. Subsequent discussion is based on the results obtained from this model.

The displacement time histories at the middle point B ($x = 100 \text{ mm}$, $y = 0 \text{ mm}$) and the end point C ($x = 200 \text{ mm}$, $y = 0 \text{ mm}$) for elastic response from SPH and FEM analyses are depicted in Fig. 10.

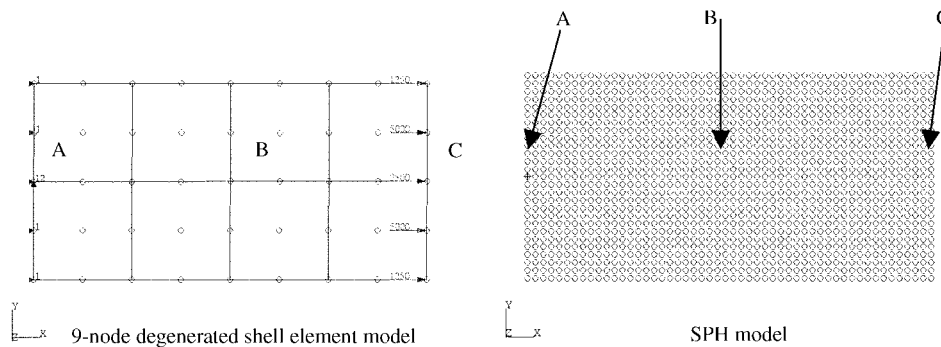


Fig. 9 FEM and SPH models of steel plate subjected to suddenly applied edge load

Table 2 Steel plate material properties and geometry data

Initial Young's modulus of elasticity	$E = 200. \times 10^3 \text{ MPa}$
Poisson's ratio	$\nu = 0.3$
Mass density	$\rho = 0.0078 \text{ g/mm}^3$
Initial yield stress	$\sigma_y = 200. \text{ MPa}$
Linear strain hardening modulus	$E^T = 2.0 \times 10^3 \text{ MPa}$
Length and width of plate	$L = 200 \text{ mm}$ and $b = 100 \text{ mm}$
Thickness	$h = 1 \text{ mm}$

Comparison of these results shows good agreement. The displacements at the middle point register about 20 μsec time-lag when compared with those at the end point. The phenomenon is also observed during the theoretical study (Drumheller 1998). The stress histories of points A and B from both SPH and FEM analyses are shown in Fig. 11. More oscillations are observed in stress histories than those of displacement. Comparison of the results from both approaches reveals that stress histories at point B are in better agreement than those at point A as the latter is located at the fixed end and hence suffered more from the reflection of stress from the edge. This stress reflection also causes more oscillation in stress histories at point A and stress at the nearest particle to the fixed edge are usually monitored and presented. It is noted that the time lag of stress wave propagation is similar to that of displacement.

Both displacement and stress histories of points B and C and/or A resulting from the elasto-plastic analyses are shown in Figs. 12 and 13 respectively. Similar to the elastic response, the displacement histories obtained from both SPH and FEM analyses, are in good agreement and the stress time histories at the middle point has better agreement than those at point A. The phenomenon is mainly due to the stress wave reflection from the constraint boundary. Time lag for results at different

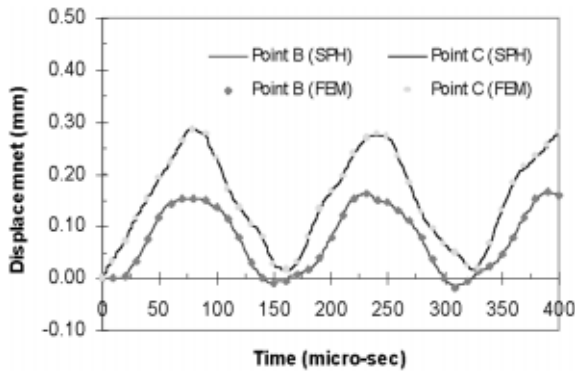


Fig. 10 Displacement histories at middle and end points for elastic case

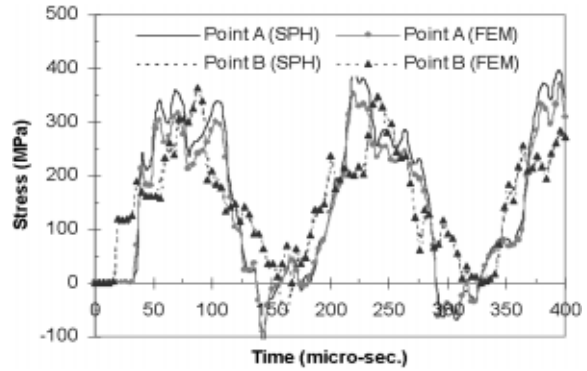


Fig. 11 Stress histories at middle and end points for elastic case

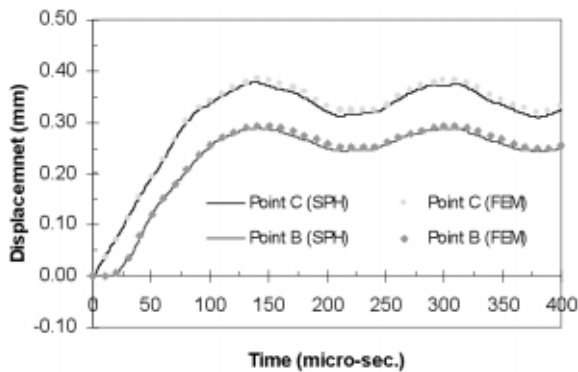


Fig. 12 Displacement histories at middle and end points for elasto-plastic case

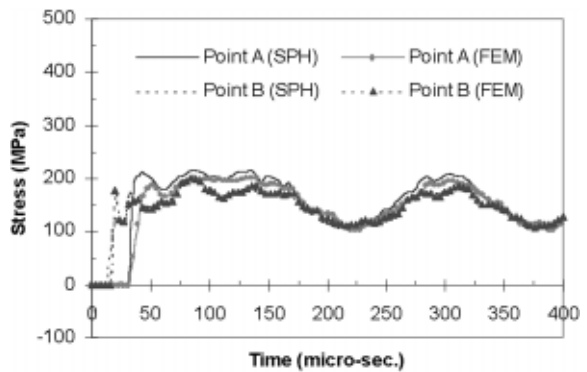


Fig. 13 Stress histories at middle and end points for elasto-plastic case

points in the domain is observed from both displacement and stress histories. This delayed time is the same as that observed earlier in the elastic case as the deformation is still elastic at this stage. However, as the stress wave reflection from the boundary reaches the observing points, the values of stress increase and the plastic deformation takes place. Plasticity effect in the material causes the stress wave propagation to slow down and hence the duration of elasto-plastic period is longer than that of the elastic case. Permanent deformation is apparent and the stress wave durations, the plastic stress amplitudes as well as the travel patterns for various points in the domain tend to converge to the same values. These phenomena are in accordance with those observed in theoretical study.

7. Conclusions

The elasto-plastic large deformation dynamic responses of structures are studied using the Smooth Particle Hydrodynamics approach. Additional stress points are introduced in the formulation to mitigate tensile instability phenomenon which is inherently present in the method. The incremental rate approach, which is effective to treat large deformation transient dynamics problems, and the leap-frog algorithm for time integration are adopted and embedded in the conventional SPH method to improve the accuracy of the results. Two examples including stress wave propagation in elastic aluminium bar and in 2-D elasto-plastic steel plate are presented to demonstrate the performance of the proposed algorithm. Numerical results obtained by the proposed SPH method compare favourably with those obtained by analytical and/or finite element method.

References

- Belytschko, T., Krongauz, Y., Dolbow, J. and Gerlach, C. (1998), "On the completeness of meshfree particle methods", *Int. J. Numer. Meth. Eng.*, **43**, 785-819.
- Benz, W. (1990), Smooth particle hydrodynamics: a review, in *the Numerical Modeling of Stellar Pulsation*, Editor J.R. Buchler. Dordrecht Kluwer.
- Chen, J.K., Beraun, J.E. and Jih, C.J. (1999a), "An improvement for tensile instability in smoothed particle hydrodynamics", *Comput. Mech.*, **23**, 279-287.
- Chen, J.K., Beraun, J.E. and Jih, C.J. (1999b), "Completeness of corrective smoothed particle method for linear elastodynamics", *Comput. Mech.*, **24**, 273-285.
- Chen, J.K., Beraun, J.E. and Jih, C.J. (2001), "A corrective smoothed particle method for elastoplastic dynamics", *Comput. Mech.*, **27**, 177-187.
- Drumheller, D.S. (1998), *Introduction to Wave Propagation in Nonlinear Fluids and Solids*, Cambridge University Press, Cambridge.
- Dyka, C.T. and Ingel, R.P. (1995), "An approach for tension instability in smoothed particle hydrodynamics (SPH)", *Comput. Struct.*, **57**, 573-580.
- Dyka, C.T., Randles, P.W. and Ingel, R.P. (1997), "Stress points for tension instability in SPH", *Int. J. Numer. Meth. Eng.*, **40**, 2325-2341.
- Gingold, R.A. and Monaghan J.J. (1977), "Smoothed particle hydrodynamics: theory and application to non-spherical stars", *Mon. Not. R. Astron. Soc.*, **181**, 375-389.
- Graff, K.F. (1975), *Wave Motion in Elastic Solids*. Oxford University Press, Oxford.
- Graffi, D. (1954), "Über den reziprozitätssatz in der dynamik elastischer körper", *Ingenieur Archiv*, **22**, 45-46.
- Hicks, D.L., Swegle, J.W. and Attaway, S.W. (1997), "Conservative smoothing stabilizes discrete-numerical instabilities in SPH materials dynamics computations", *Applied Mathematics and Computation*, **85**(2-3), 209-226.

- Hockney, R.W. and Eastwood, J.W. (1981), *Computer Simulation Using Particles*, McGraw-Hill., New York.
- Johnson, G.R., Beissel, S.R. (1996), "Normalized smoothed functions for SPH impact computations", *Int. J. Numer. Meth. Eng.*, **39**, 2725-2741.
- Libersky, L.D. and Petschek, A.G. (1991), "Smooth particle hydrodynamics with strength of materials", In: *Advances in the Free-Lagrange Method*, Editors H.E. Trease, M.J. Fritts and W.P. Crowley, Springer, New York, 248-257.
- Libersky, L.D., Petschek, A.G., Carney, T.C., Hipp, J.R. and Allahdadi, F.A. (1993), "High strain Lagrangian hydrodynamics, a three dimension SPH code for dynamic material response", *J. Comp. Phys.*, **109**, 67-75.
- Lucy, L.B. (1977), "A numerical approach to the testing of the fission hypothesis", *Astronom. J.*, **82**, 1013-1024.
- Molenkamp, F. (1986), "Limits to the Jaumann stress rate", *Int. J. Num. Anal. Meth. Geomech.*, **10**, 151-176.
- Monaghan, J.J. (1985), "Particle methods for hydrodynamics", *J. Comp. Phys. Rep.*, **3**, 71-124.
- Monaghan, J.J. (1989), "On the problem of penetration in particle methods", *J. Comp. Phys.*, **82**, 1-20.
- Monaghan, J.J. and Gingold, R.A. (1983), "On the problem of hydrodynamics in particle methods", *J. Comp. Phys.*, **52**, 374.
- Owen, D.R.J. and Hinton, E. (1980), *Finite Elements In Plasticity: Theory and Practice*, Pineridge Press, Swansea, UK.
- Randles, P.W. and Libersky, L.D. (1996), "Smoothed particle hydrodynamics: Some recent improvements and applications", *Comput. Methods Appl. Mech. Engrg.*, **139**, 375-408.
- Randles, P.W. and Libersky, L.D. (2000), "Normalized SPH with stress points", *Int. J. Numer. Meth. Eng.*, **48**, 1445-1662.
- Swaddiwudhipong, S. and Liu, Z.S. (1996), "Dynamic response of large strain elasto-plastic plate and shell structures", *Thin Walled Structures*, **26**(4), 223-239.
- Swegle, J.W. and Attaway, S.W. (1995), "On the feasibility of using smoothed particle hydrodynamics for underwater explosion calculations", *Comput. Mech.*, **17**, 151-168.
- Swegle, J.W., Hicks, D.L. and Attaway, S.W. (1995), "Smoothed particle hydrodynamics stability analysis", *J. Comp. Phys.*, **116**, 123-134.